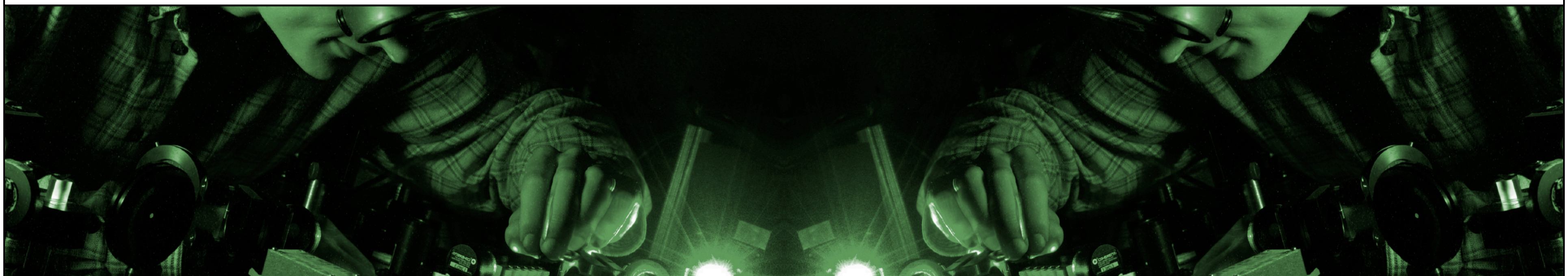

November 13, 2009

Gaussian States and Quantum Imaging

Jeffrey H. Shapiro and Franco N. C. Wong

Research sponsored by the U.S. Army Research Office,
the Defense Advanced Research Projects Agency, and
the W. M. Keck Foundation Center for Extreme Quantum Information theory

Optical and Quantum Communications Group

RESEARCH LABORATORY OF ELECTRONICS
Massachusetts Institute of Technology

www.rle.mit.edu/qoptics

Gaussian States and Quantum Imaging

- Gaussian states
  - classical versus quantum
- Optical coherence tomography (OCT)
  - conventional versus quantum versus phase-conjugate OCT
- Ghost imaging
  - signal-to-noise ratio and image-acquisition time
- Nonlocal dispersion cancellation
  - biphoton versus mixed-state entangled versus classically correlated
- Sub-Rayleigh imaging
  - improving spatial resolution with classical-state light

Unified Gaussian-State Framework

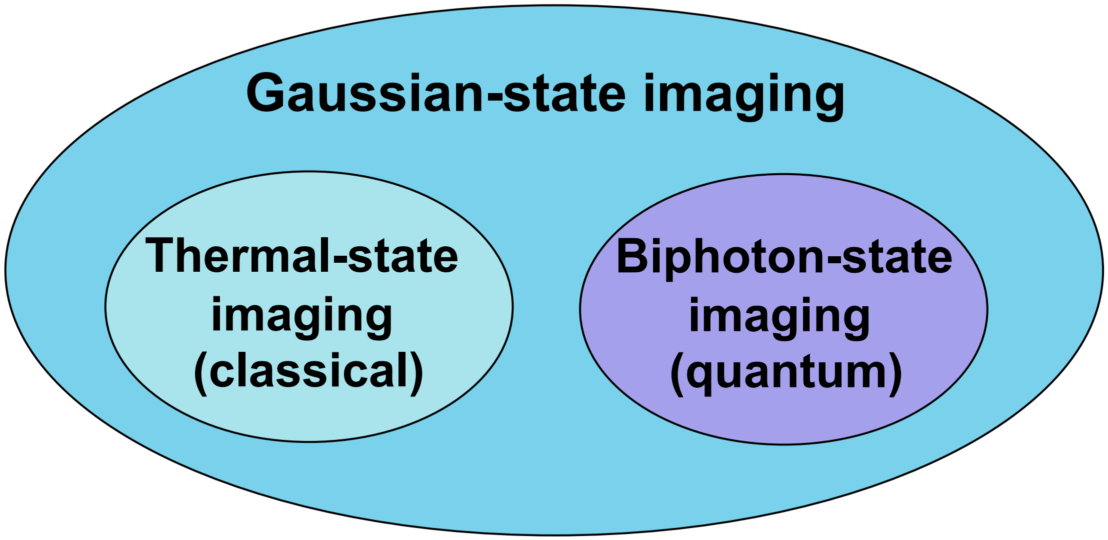

- Gaussian states include…
  - laser light, LED light, sunlight, i.e., "classical states"
  - low-flux biphoton output from SPDC, viz., a "quantum" state
- Gaussian states are…
  - characterized by their mean values and coherence functions
  - closed under linear transformations like free-space diffraction

Properties of Phase-Insensitive Coherence

- Phase-insensitive coherence at source

$$\langle \hat{E}_0^\dagger(\boldsymbol{\rho}_1, t_1)\hat{E}_0(\boldsymbol{\rho}_2, t_2)\rangle = \frac{2P}{\pi a_0^2} e^{-(|\boldsymbol{\rho}_1|^2+|\boldsymbol{\rho}_2|^2)/a_0^2 - |\boldsymbol{\rho}_1-\boldsymbol{\rho}_2|^2/2\rho_0^2} e^{-(t_1-t_2)^2/2T_0^2}$$

- spatial coherence is quasiplanatic

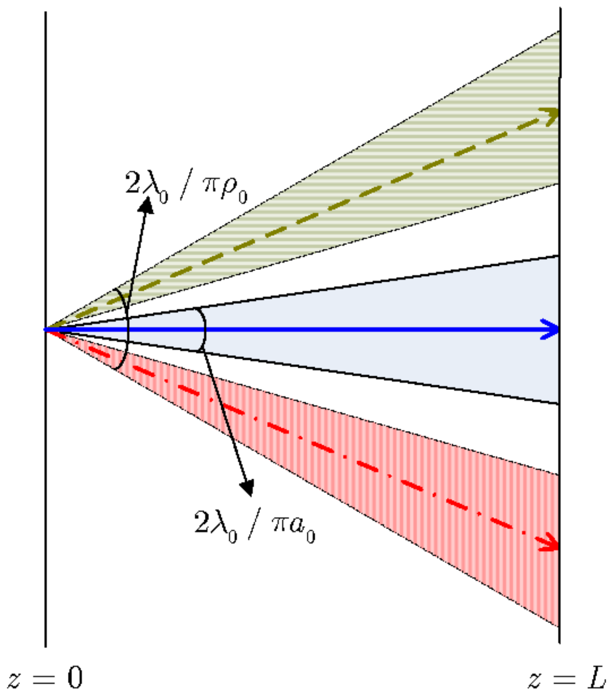

- temporal coherence is monochromatic

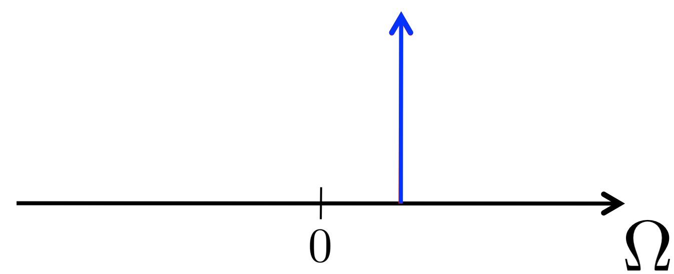

- produces second-order interference

Properties of Phase-Sensitive Coherence

- Phase-sensitive coherence at source

$$\langle \hat{E}_0(\boldsymbol{\rho}_1, t_1)\hat{E}_0(\boldsymbol{\rho}_2, t_2)\rangle = \frac{2P}{\pi a_0^2} e^{-(|\boldsymbol{\rho}_1|^2+|\boldsymbol{\rho}_2|^2)/a_0^2 - |\boldsymbol{\rho}_1-\boldsymbol{\rho}_2|^2/2\rho_0^2} e^{-(t_1-t_2)^2/2T_0^2}$$

- spatial coherence is quasibiplanatic

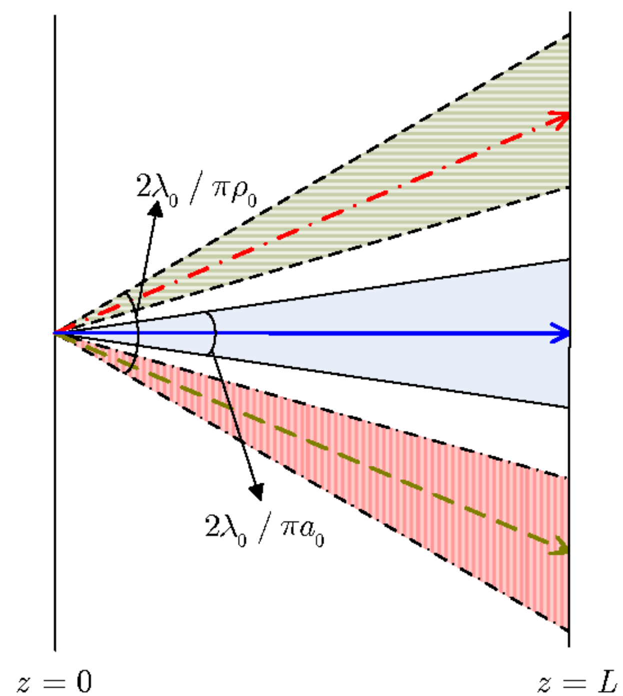

- temporal coherence is bichromatic

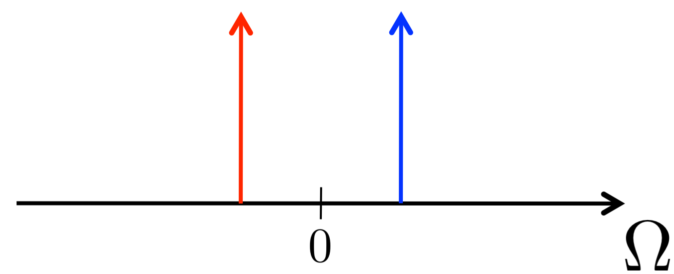

- does *not* produce second-order interference

Erkmen & Shapiro, Proc SPIE 6305, 6305G (2006)

Optical Coherence Tomography

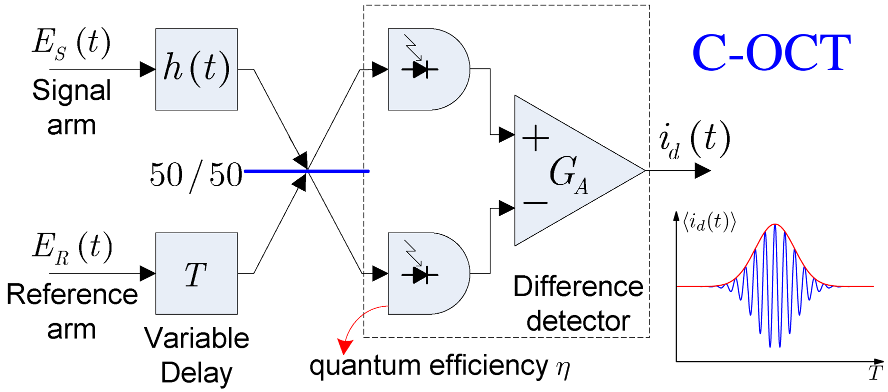

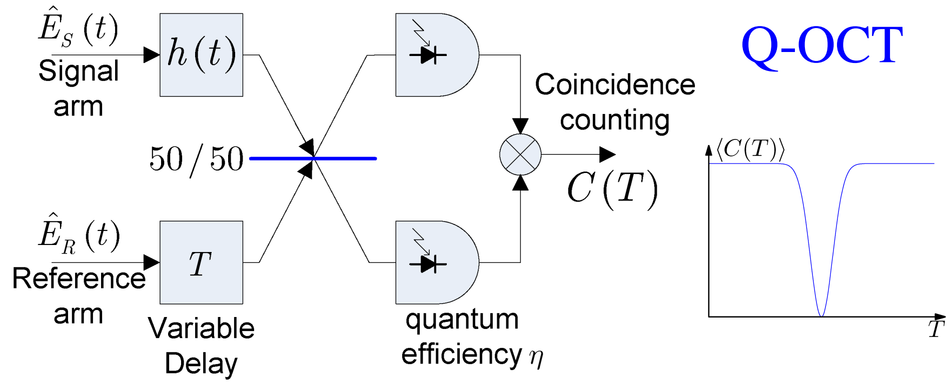

Abouraddy *et al.*, PRA 65, 053817 (2002); Nasr *et al.*, PRL 91, 083601 (2003)

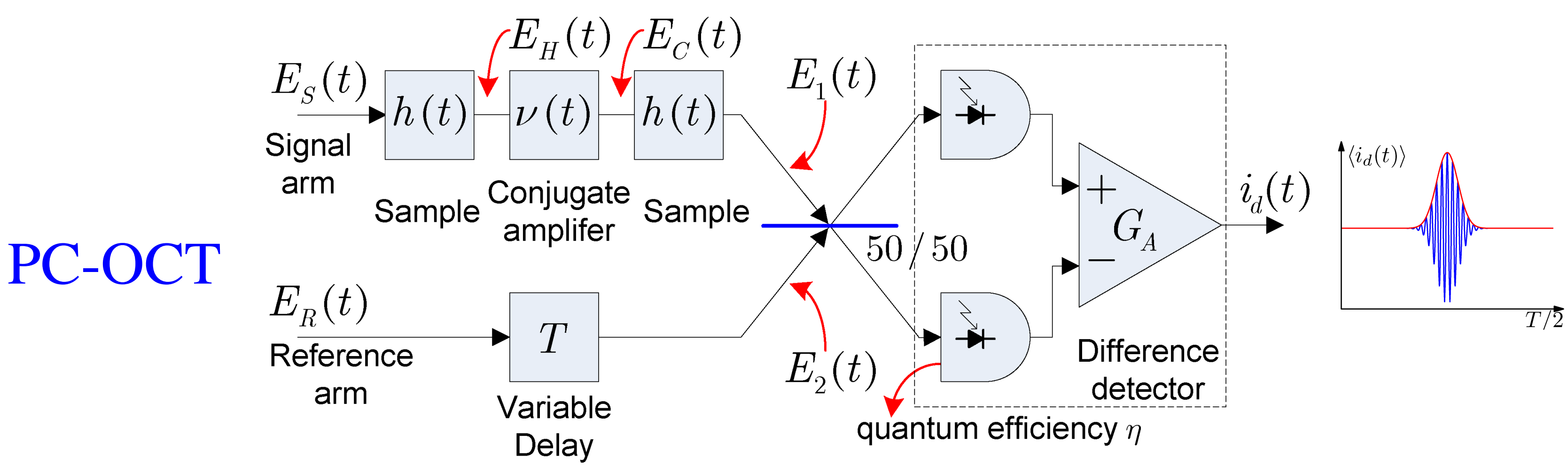

Erkmen & Shapiro, PRA 74, 041601(R) (2006)

Mean Signatures from a Single Mirror

- Gaussian source power spectrum, $S(\Omega) = P_S\sqrt{2\pi/\Omega_S^2}\,e^{-\Omega^2/2\Omega_S^2}$
- Broadband conjugator, $V(\Omega) \approx V = |V|e^{i\theta_V}$
- Weakly reflecting mirror, $H(\Omega) = re^{i[(\omega_0+\Omega)T_0+b\Omega^2/2]}$, $|r| \ll 1$.

$$\langle i_d(t)\rangle \propto e^{-\Omega_S^2(T_0-T)^2/2(1+\Omega_S^4 b^2)}\cos(\omega_0(T-T_0)-\theta_r)$$

$$\langle C(T)\rangle \propto (1-e^{-2(T_0-T)^2\Omega_S^2})$$

$$\langle i_d(t)\rangle \propto e^{-2\Omega_S^2(T_0-T/2)^2}\cos(\omega_0 T-\theta_V)$$

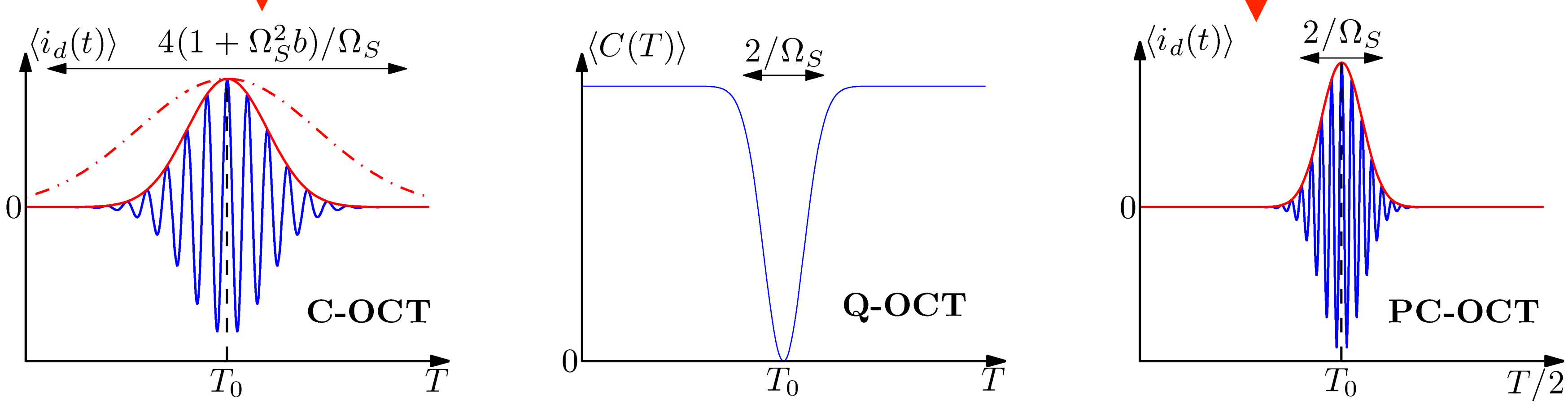

Erkmen & Shapiro, PRA 74, 041601(R) (2006)

Phase-Conjugate OCT Experiment

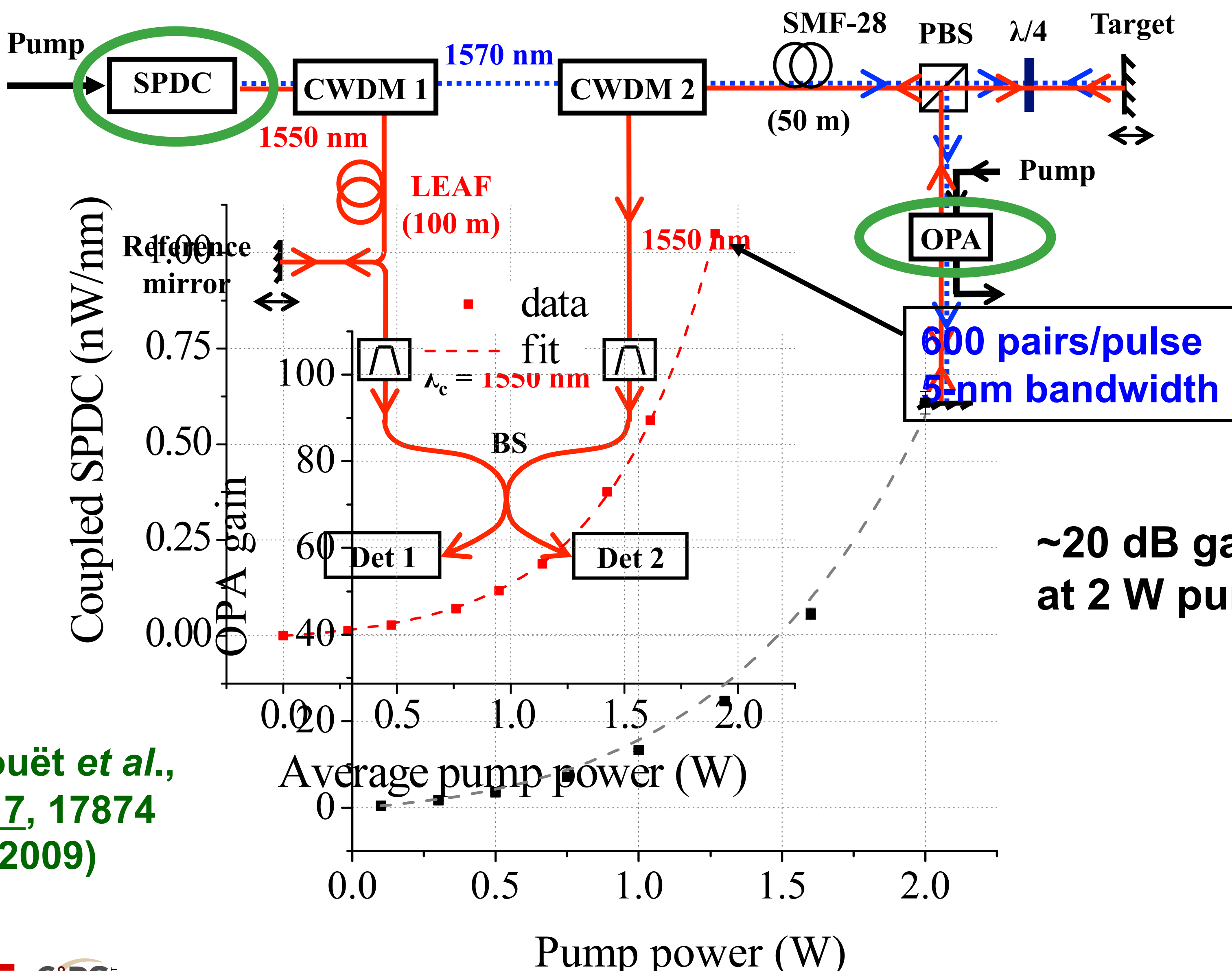

~20 dB gain at 2 W pump

Le Gouët *et al.*, OE <u>17</u>, 17874 (2009)

Axial Resolution and Dispersion Cancellation

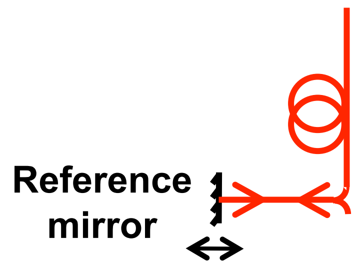

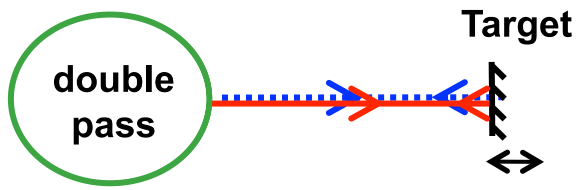

2x axial resolution enhancement: $\Delta z_T = 450\ \mu m$
$\Delta z_R \approx 2(\Delta z_T)$

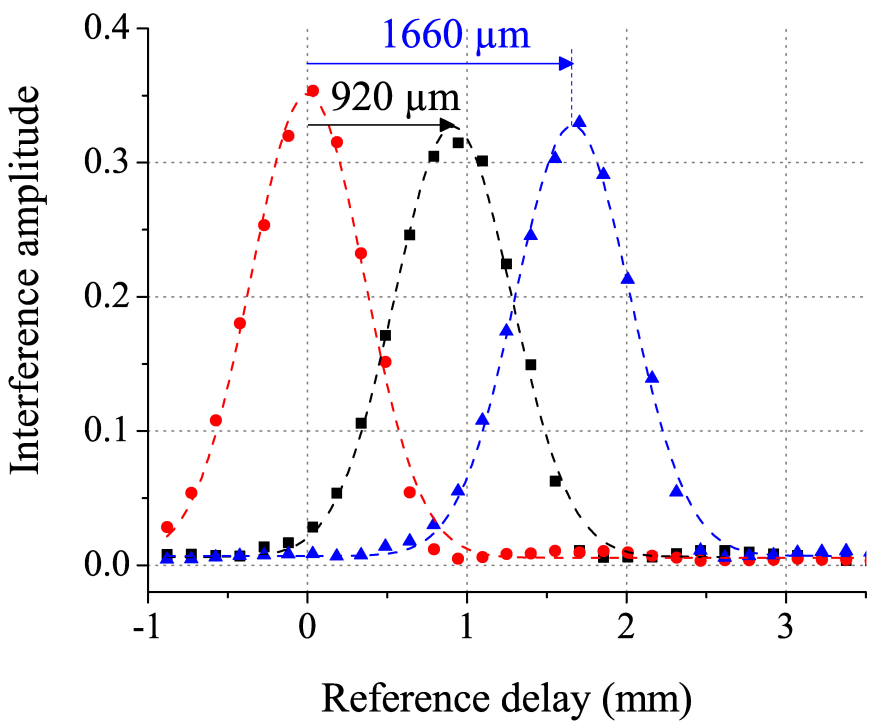

Interference envelope width

Measured (FWHM) = 890 µm

Width would be 3.0 mm without signal dispersion cancellation

Le Gouët *et al.*, submitted (2009)

Optical Coherence Tomography Discussion

- Improvements in Q-OCT and PC-OCT are due to phase-sensitive coherence between signal and reference beams
- Entanglement not the key property yielding the benefits
- Q-OCT: $H^*(-\Omega)H(\Omega)$ obtained from an actual sample illumination and a virtual sample illumination
- PC-OCT: $H^*(-\Omega)H(\Omega)$ obtained via two sample illuminations
- Double-pass conventional illumination can achieve the 2x improvement in axial resolution but at the expense of 2x resolution loss due to dispersion
- PC-OCT combines Q-OCT's resolution and dispersion cancellation with C-OCT's high SNR

Four Types of Active Ghost Imaging

Biphoton ghost imaging

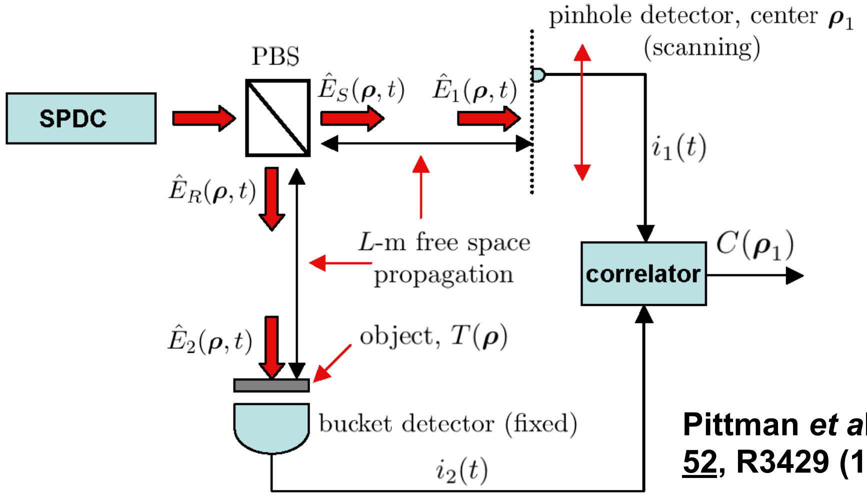

Pittman *et al.*, PRA <u>52</u>, R3429 (1995)

Pseudothermal ghost imaging

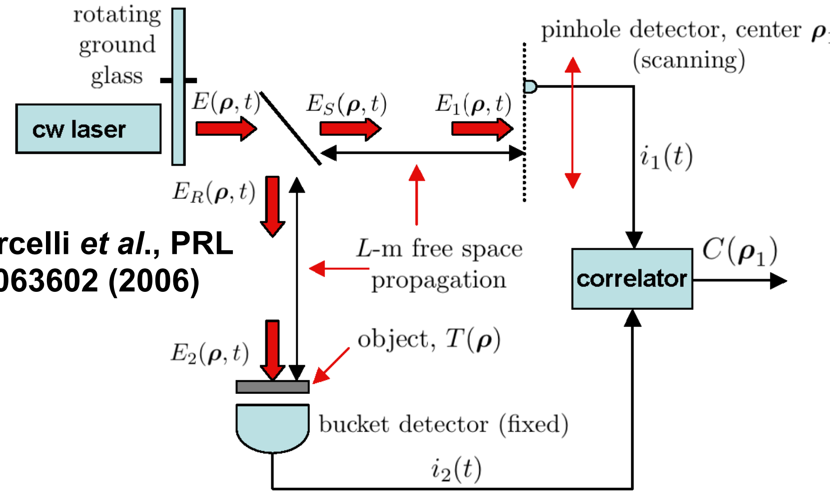

Scarcelli *et al.*, PRL <u>77</u>, 063602 (2006)

Spatial light modulator ghost imaging

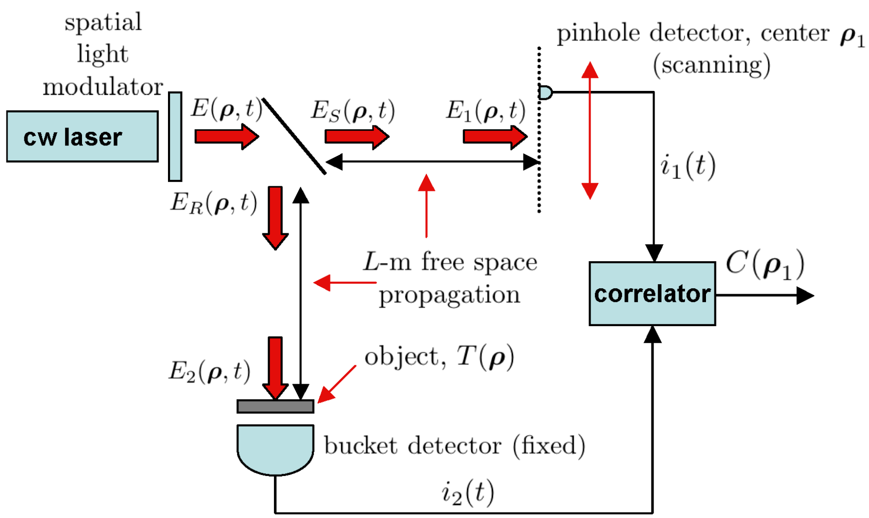

Computational ghost imaging

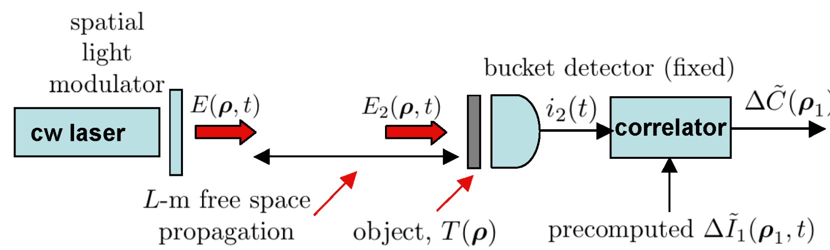

Erkmen & Shapiro, PRA <u>77</u>, 043809 (2008);
Erkmen & Shapiro, PRA <u>79</u>, 023833 (2009);
Shapiro, PRA <u>78</u>, 061802(R) (2008).

Gaussian-State Image Resolution and Contrast

- Far-field operation:

  biphoton $k_0 a_0^2/2L \ll 1$, pseudothermal $k_0 a_0 \rho_0/2L \ll 1$

- Object within field of view:

  biphoton $\sqrt{2}\lambda_0 L/\pi\rho_0$, pseudothermal $\lambda_0 L/\pi\rho_0$

- Photocurrent cross-correlation functions

$$\begin{aligned}\langle C(\boldsymbol{\rho}_1)\rangle &= q^2\eta_1\eta_2 A_1\left(\frac{2P}{\pi a_L^2}\right)^2\Bigg[\overbrace{\int_{\mathcal{A}_2} d\boldsymbol{\rho}\,|T(\boldsymbol{\rho})|^2}^{\textbf{background}}\\ &+ \mathcal{C}_\pm \underbrace{\int_{\mathcal{A}_2} d\boldsymbol{\rho}\, e^{-|\boldsymbol{\rho}_1 \pm \boldsymbol{\rho}|^2/\rho_L^2}|T(\boldsymbol{\rho})|^2}_{\textbf{ghost image}}\Bigg]\end{aligned}$$

coherence radius $\rho_L = \lambda_0 L/\pi a_0$

biphoton $\mathcal{C}_+ \gg 1$, pseudothermal $\mathcal{C}_- = 1$

Erkmen & Shapiro, PRA 77, 043809 (2008)

Signal-to-Noise Ratio Analysis

- Time average used to approximate ensemble average
- Source coherence time: T_0
- Photodetector bandwidth: Ω_B
- Cross-correlation integration time: T_I
- Broadband biphoton imaging: $\Omega_B T_0 \ll 1, \Omega_B T_I \gg 1$
- Narrowband pseudothermal imaging: $\Omega_B T_0 \gg 1, T_0 \ll T_I$
- SNR analysis done via Gaussian moment factoring

Signal-to-Noise Ratio Behavior

Nonclassical Source

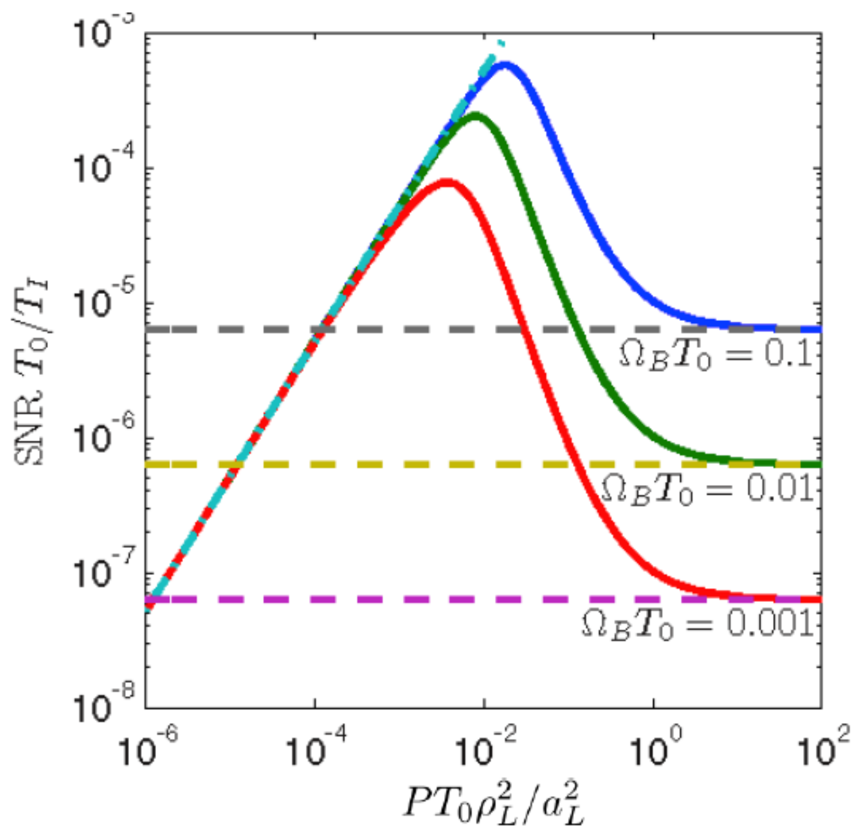

Pseudothermal Source

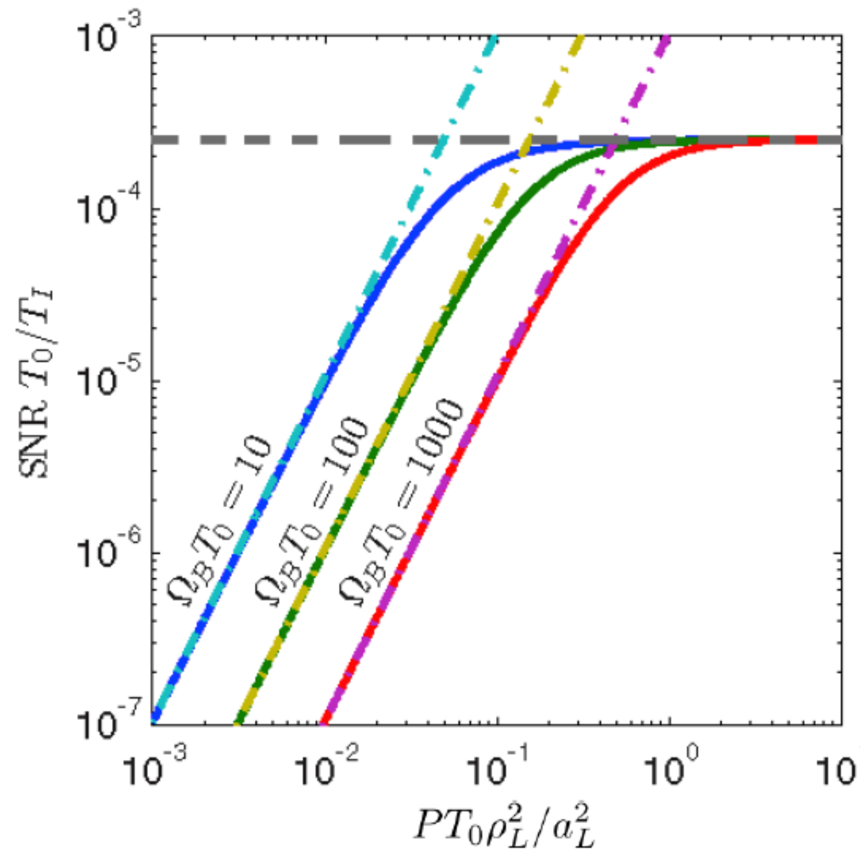

Erkmen & Shapiro, PRA 79, 023833 (2009)

Far-Field Propagation Image-Acquisition Times

- Broadband biphoton source
  - $T_I^{(q)}$ = time to achieve target SNR value
- Narrowband, high-brightness, pseudothermal source
  - $T_I^{(c)}$ = time to achieve target SNR value
- For the same target SNR values

$$\frac{T_I^{(q)}}{T_I^{(c)}} = \underbrace{\frac{\sqrt{2\pi^3}|T(\boldsymbol{\rho}_1)|^4}{\eta^2|T(-\boldsymbol{\rho}_1)|^2}}_{\sim 8|T|^2/\eta^2} \underbrace{\frac{\rho_L^2}{A'_T}}_{10^{-4}} \underbrace{\frac{\rho_L^2}{A_1}}_{10^2} \underbrace{\frac{a_0^2}{P^{(q)}T_0^{(q)}\rho_0^2}}_{\sim 10^6} \underbrace{\frac{T_0^{(q)}}{T_0^{(c)}}}_{10^{-6}}$$

an example / another example

$$\approx 8 \times 10^{-2}|T|^2/\eta^2$$

$$\approx 8 \times 10^{-3}|T|^2/\eta^2$$

Ghost Imaging Discussion

- Gaussian-state framework unifies ghost-imaging analyses
- Far-field resolution behavior is identical for biphoton and pseudothermal sources
- Biphoton source enjoys slight field-of-view advantage over pseudothermal source
- Biphoton source enjoys significant contrast advantage over pseudothermal source
- Broadband biphoton source *may* have significant image-acquisition time advantage over narrowband, bright, pseudothermal source

Nonlocal Dispersion Cancellation

- Biphoton illumination enjoys cancellation of group-velocity dispersion with opposite signs in nonlocal manner

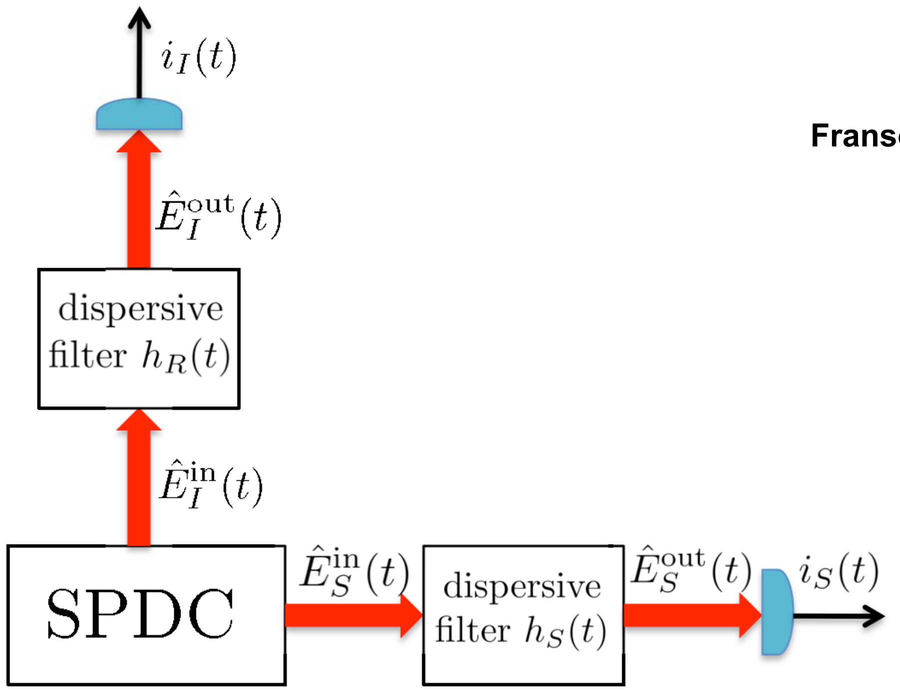

Franson, PRA 45, 3126 (1992)

- Classical-state light — even classical *phase-sensitive* light — cannot reproduce this phenomenon

Franson, arXiv:0907.5196 [quant-ph];
Franson, arXiv:0909.2846 [quant-ph]

Dispersion Cancellation with Phase-Sensitive Light

- Consider phase-sensitive Gaussian state light source

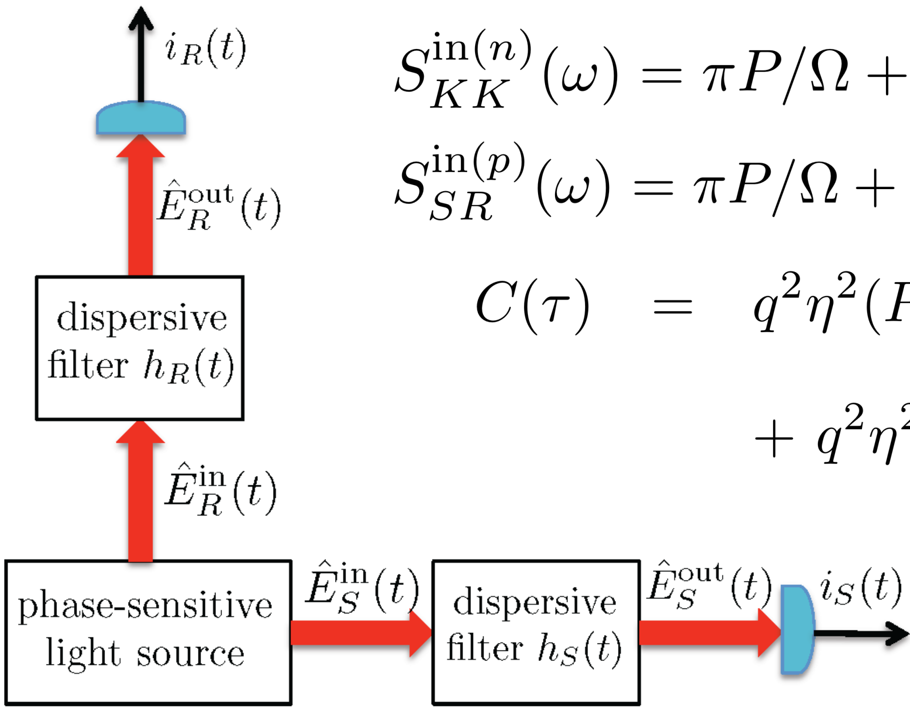

$$S_{KK}^{\text{in}(n)}(\omega) = \pi P/\Omega + (G-1), \text{ for } |\omega| \le \Omega,\ K = S, R$$

$$S_{SR}^{\text{in}(p)}(\omega) = \pi P/\Omega + i\sqrt{\pi P/\Omega}, \text{ for } |\omega| \le \Omega$$

$$\begin{aligned} C(\tau) &= q^2\eta^2(P + (G-1)\Omega/\pi)^2 \\ &\quad + q^2\eta^2(P^2 + P\Omega/\pi)\left(\frac{\sin(\Omega\tau)}{\Omega\tau}\right)^2 \end{aligned}$$

- Coincidence peak has same width but background increases as state progresses from pure-entangled to mixed-entangled to classical-maximally-correlated to classical-partially-correlated

Shapiro, arXiv:0909.2514 [quant-ph]

Ladar Imaging: Monostatic Operation

- Diffraction-limited transmitter:

  $$\text{power } P_T, \text{ diameter } D_T, \text{ wavelength } \lambda$$

- Diffraction-limited receiver: $\text{diameter } D_R$
- Speckle-averaged focal-plane intensity

$$I(\boldsymbol{\theta}' f) = \frac{4P_T}{\pi D_T^2} \underbrace{(\mathcal{F}_T\mathcal{F}_R)}_{\text{Fresnel-number product}}{}^2 \int \mathrm{d}\boldsymbol{\theta}\, \underbrace{[p_T(\boldsymbol{\theta})}_{\text{Transmitter antenna-pattern}} \overbrace{\mathcal{T}(\boldsymbol{\theta}L)}^{\text{Target intensity-reflectivity}}] \underbrace{p_R(\boldsymbol{\theta}' - \boldsymbol{\theta})}_{\text{Receiver antenna-pattern}}$$

$$L = \text{target range}, f = \text{receiver focal length}$$

$$p_x(\boldsymbol{\theta}) = \left(\frac{2J_1(\pi D_x|\boldsymbol{\theta}|/\lambda)}{\pi D_x|\boldsymbol{\theta}|/\lambda}\right)^2 = \text{ point-spread function}$$

Floodlight Illumination with Array Photodetection

- When entire target is illuminated

$$I(\boldsymbol{\theta}' f) \approx \frac{4P_T}{\pi D_T^2}(\mathcal{F}_T\mathcal{F}_R)^2 \int \mathrm{d}\boldsymbol{\theta}\, \mathcal{T}(\boldsymbol{\theta} L) p_R(\boldsymbol{\theta}' - \boldsymbol{\theta})$$

- Resolution is the receiver's Rayleigh limit

$$|\Delta\boldsymbol{\theta}|L = 1.22\lambda L/D_R \text{ at first zero of } p_R(\Delta\boldsymbol{\theta})$$

when not limited by the photodetection array

Pinpoint Illumination with Precision Raster Scan

- When we illuminate a sequence of angles $\{\boldsymbol{\theta}_i\}$ in a precision raster scan, the received power is

$$P_R = \int \mathrm{d}\boldsymbol{\theta}' f^2\, I(\boldsymbol{\theta}' f) = \frac{4P_T}{\pi D_T^2} \mathcal{F}_T^2 \frac{\pi D_R^2}{4} \int \mathrm{d}\boldsymbol{\theta}\, p_T(\boldsymbol{\theta}_i - \boldsymbol{\theta}) \mathcal{T}(\boldsymbol{\theta} L)$$

  for illumination at $\boldsymbol{\theta}_i$

- If $D_T \gg D_R$ we resolve the target at the transmitter's Rayleigh limit

$$|\Delta\boldsymbol{\theta}|L = 1.22\lambda L / D_T \text{ at first zero of } p_T(\Delta\boldsymbol{\theta})$$

Sub-Rayleigh Imaging with Classical-State Light

- Illuminate a randomly-chosen $\boldsymbol{\theta}_i$ using $D_T \gg D_R$
- Probability of N-photon coincide at $(\boldsymbol{r}_k, t_k)$ averaged over probability density $p(\boldsymbol{\theta}_i)$ for $\boldsymbol{\theta}_i$

$$P_N(\boldsymbol{r}_k, t_k) \approx$$

$$\int \mathrm{d}\boldsymbol{\theta}_i \, p(\boldsymbol{\theta}_i) \left(\frac{\eta P_T T_d}{\hbar\omega} \frac{A_d}{L^2} \mathcal{F}_R^2 \mathcal{T}(\boldsymbol{\theta}_i L) p_R(\boldsymbol{r}_k/f - \boldsymbol{\theta}_i) \right)^N \ll 1$$

- Resolution exceeds the receiver's Rayleigh limit

Giovannetti et al., PRA 79, 013827 (2009)

Sub-Rayleigh Imaging

- Point-spread function comparison

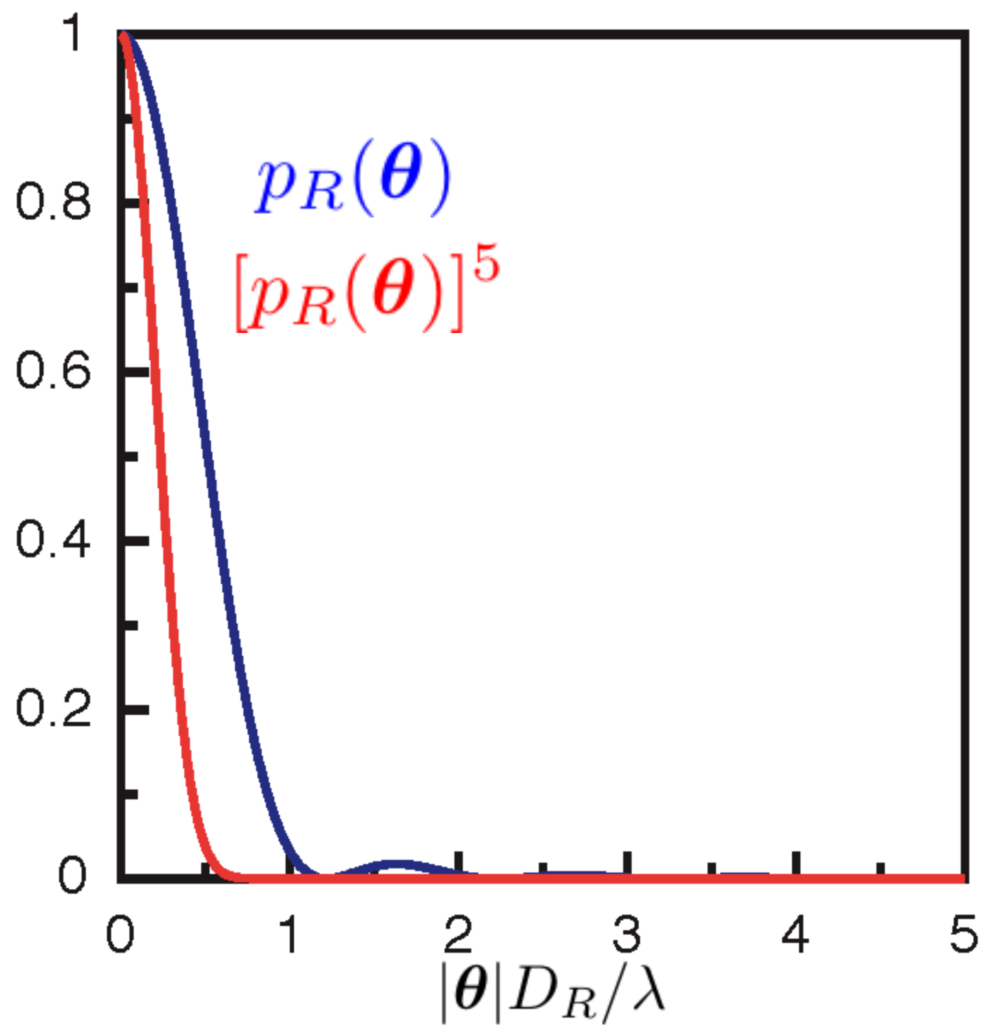

Sub-Rayleigh Imaging

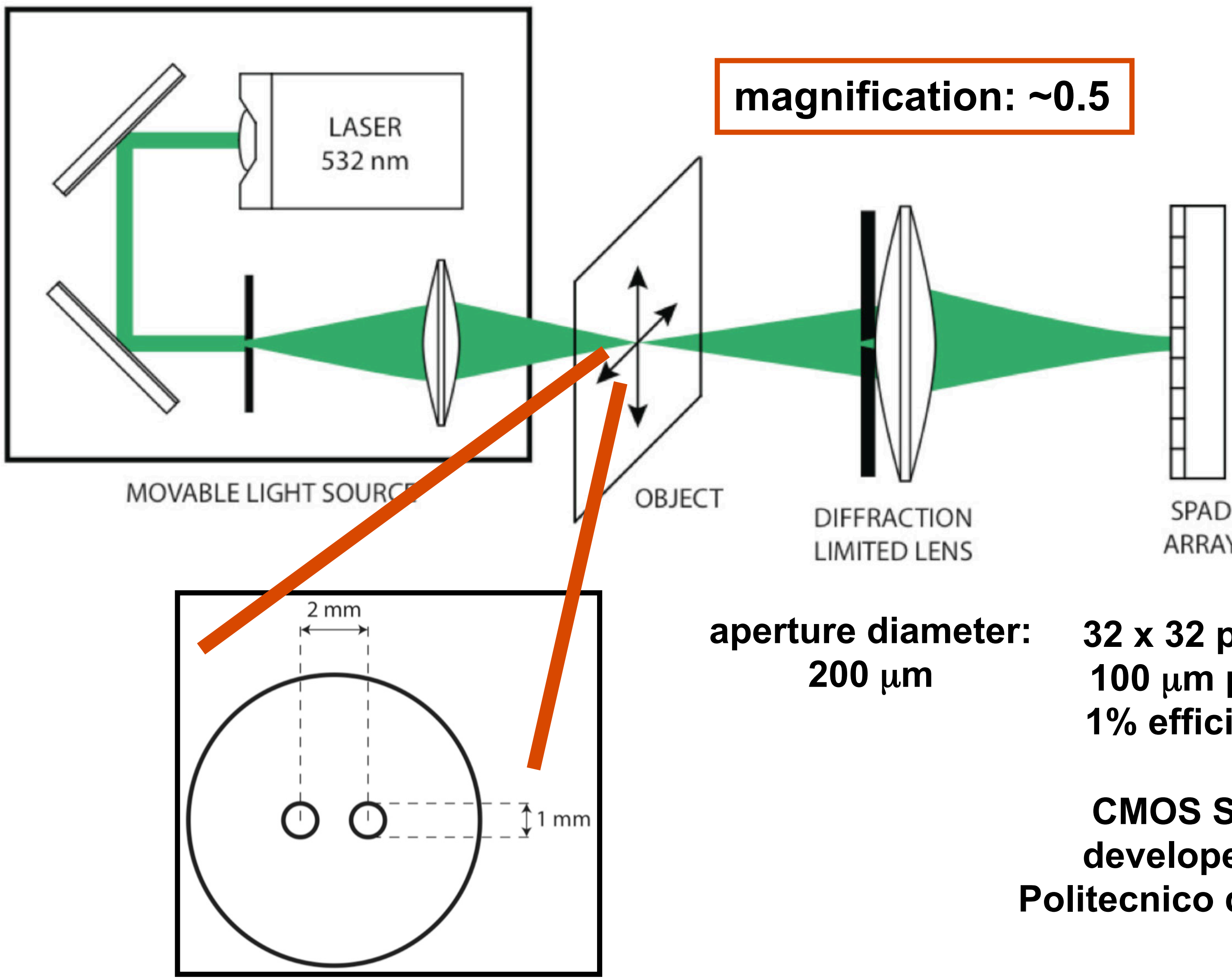

magnification: ~0.5

aperture diameter:
200 μm

32 x 32 pixels
100 μm pitch
1% efficiency

CMOS SPAD
developed by
Politecnico di Milano

beam diameter: 40 μm

CMOS SPAD Array

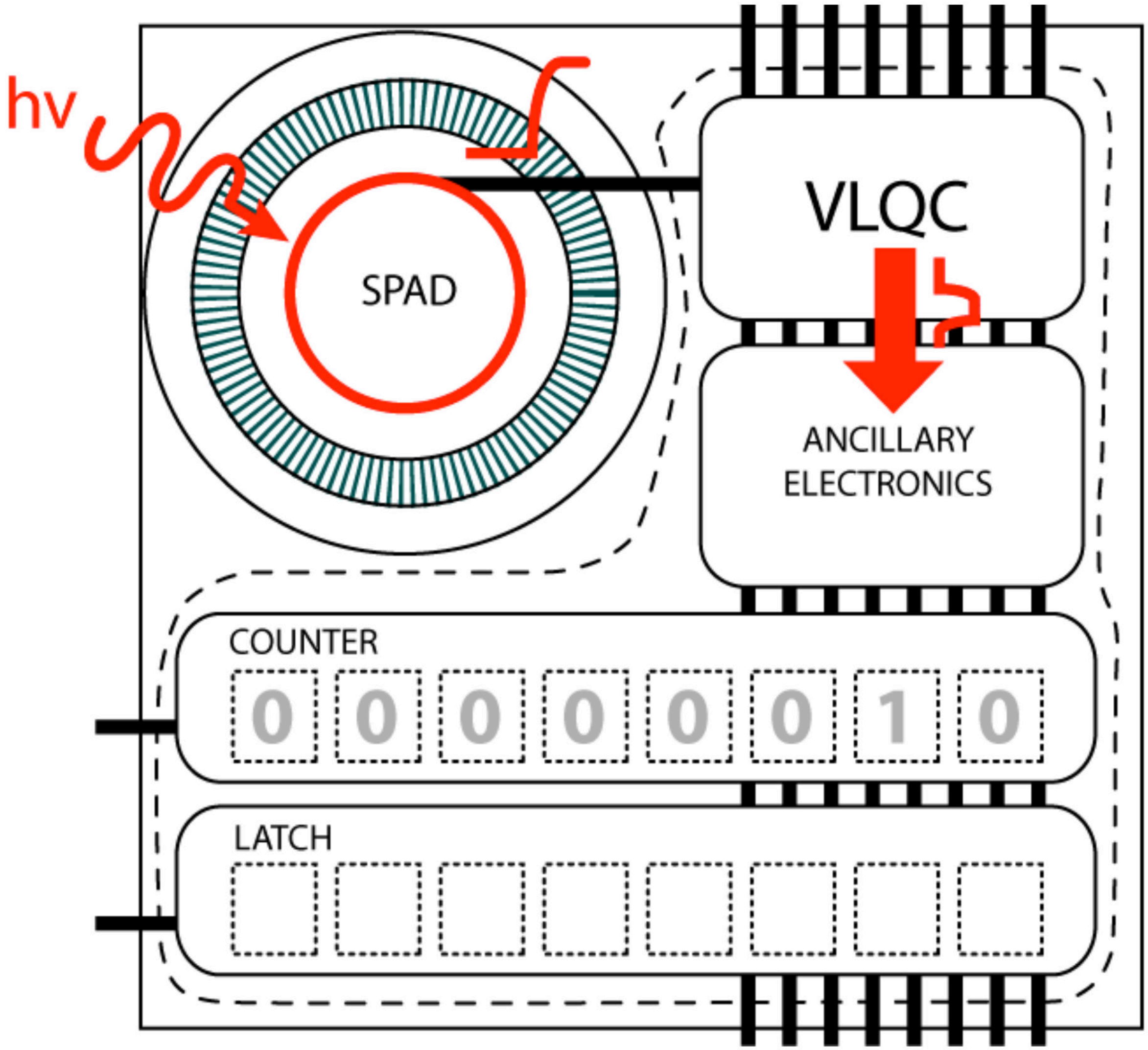

Sub-Rayleigh Imaging: Preliminary Results

Random manual laser beam scanning at object

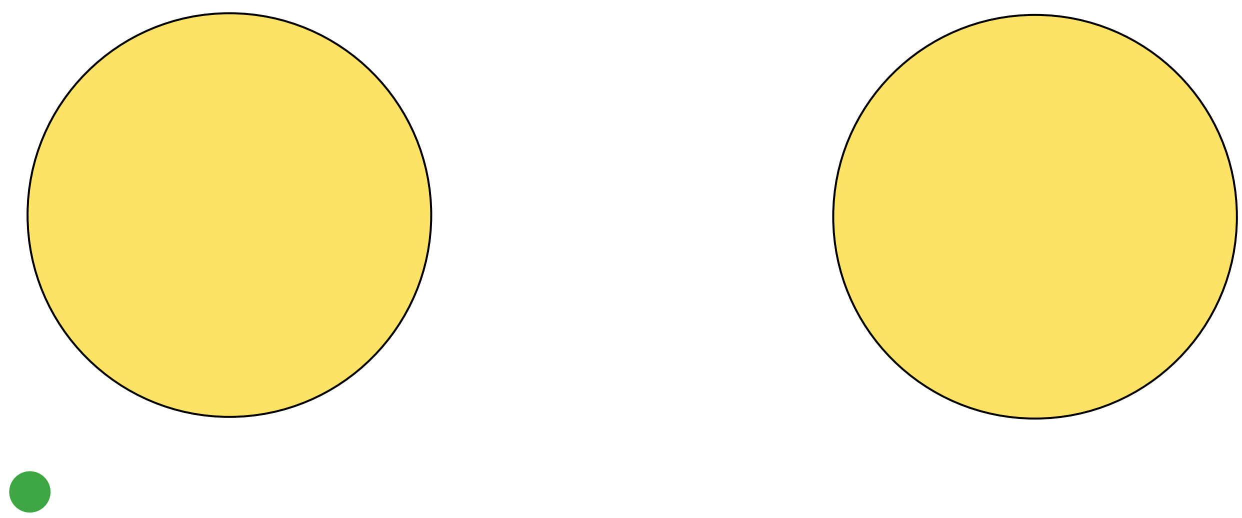

Sub-Rayleigh Imaging: Preliminary Results

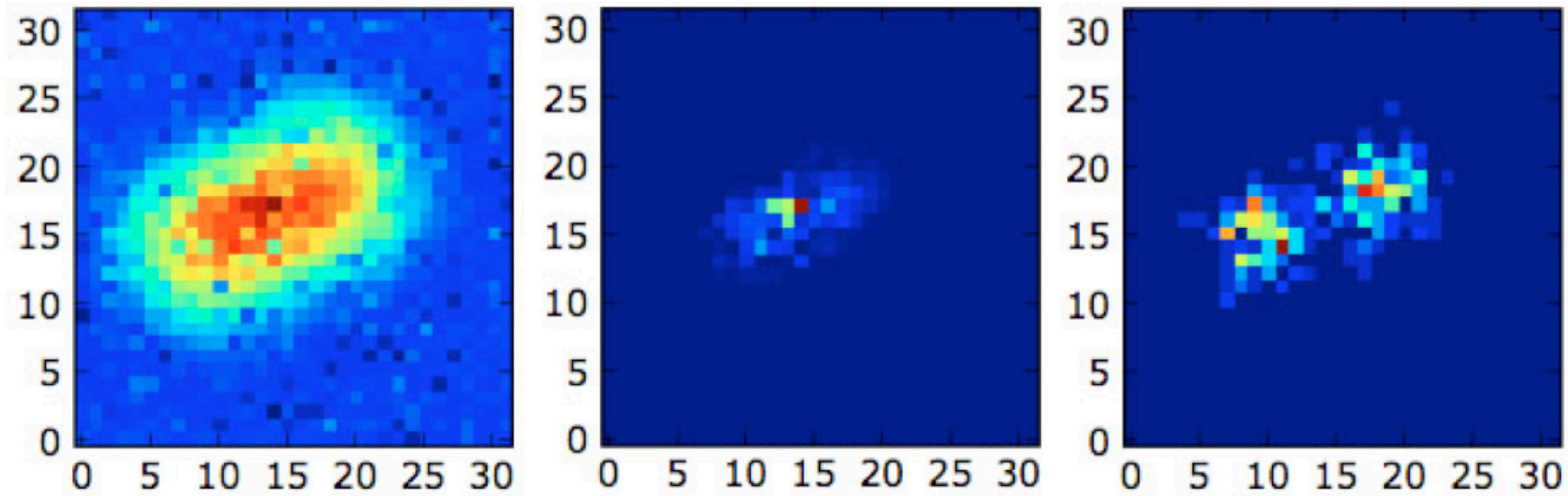

Accumulate data from all measurement frames	**Post-processing: *N*-th power of Left-panel data (*N*=10)**	**Post-processing: (1) for each frame, set pixel value to 1 if exactly *N* counts; otherwise set to 0 (2) sum all post-processed frames (*N*=10)**

Sub-Rayleigh Imaging Discussion

- Transmitter and receiver antenna patterns combine to determine image resolution of an active sensor
- *N*-photon coincidence counting does not improve resolution with floodlight illumination
- Random scanning with high-resolution beam yields resolution improvement with *N*-photon coincidence counting

$$|\Delta\boldsymbol{\theta}| \sim |\Delta\boldsymbol{\theta}_{\mathrm{Rayleigh}}|/\sqrt{N}$$

- Efficiency issues exist

Gaussian States and Quantum Imaging

- Gaussian states:
  - include the principal sources of interest for imaging
  - phase-insensitive and phase-sensitive correlations contrasted
- Phase-conjugate optical coherence tomography
  - offers the advantages of Q-OCT and C-OCT
  - proof-of-principle experiment completed
- Ghost imaging
  - SNR analysis biphoton and pseudothermal cases completed
  - experiments on SLM and computational ghost imaging beginning
- "Nonlocal" dispersion cancellation
  - phase-sensitive coherence propagation is root cause of this effect
- Sub-Rayleigh imaging
  - classical-state imaging with random scanning can exceed the Rayleigh limit of the receiver
  - preliminary experimental results support the theory

PC-OCT for Layer Measurement

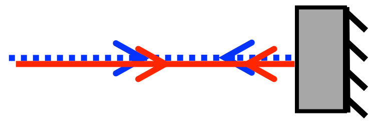

Partially reflecting household mirror

thickness: 1.74 mm
n ~ 1.5

glass-Al interface

air-glass interface

double reflections in glass

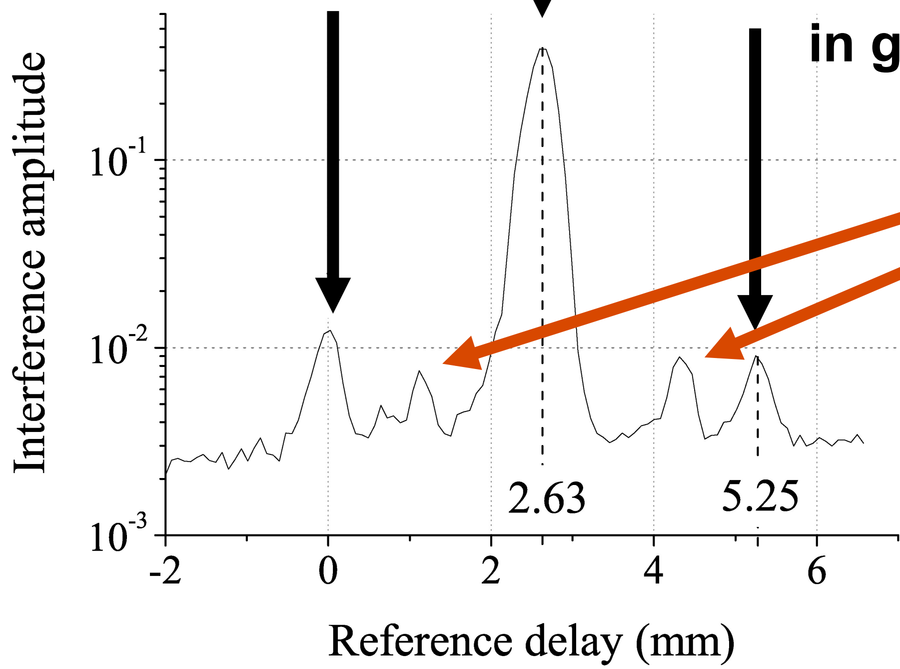

spurious signals (interference filter)

Le Gouët *et al.*, submitted (2009)